Delamination Kinetics of Thin Film Poly(acrylate) Model Coatings Prepared by Surface Initiated Atom Transfer Radical Polymerization on Iron

Jesús S. Mondragón-Ochoa,[1] Abdulrahman Altin,[1] Julian Rechmann,[1] and Andreas Erbe[1,2,z]

[1] *Max-Planck-Institut für Eisenforschung GmbH, 40237 Düsseldorf, Germany*
[2] *NTNU, Norwegian University of Science and Technology, Department of Materials Science and Engineering, 7491 Trondheim, Norway*

Living radical polymerization is often considered as an unsuitable method of surface modification for reactive metals such as iron. Necessary noble metal catalyst systems may react with the surface to be modified, causing deactivation of the catalyst. Here, surface-initiated atom transfer radical polymerization (SI-ATRP) using the typical Cu^{I}-based catalyst was used to synthesize well-defined poly(methyl methacrylate) thin films grafted on iron. Alkoxy- and chloro-silane initiators were anchored to the metal surface via Si-O-Fe bonds in a metal pretreatment step, yielding a thin cross-linked multilayer sol/gel coating. Except for the precursor's leaving group, the resulting 10s of nm thick polymer layers were almost identical. Assessment of the delamination kinetics of the model coatings by scanning Kelvin probe (SKP) showed the average delamination to be ≈40 % lower in the systems with alkoxy-precursor compared to those with chloro-precursor. In addition, the spread of the measured delamination rates decreased to 1/3 in the alkoxy system, despite identical polymers. The higher delamination rate in the case of chloro-precursors was attributed to residual chloride at the interface. Initiator surface coverage differences may also contribute to stability differences. The ATRP-Cu^{I}-catalyst is consequently also suitable for surface modification of non-noble metals after appropriate pretreatment.
 [DOI: 10.1149/2.0241816jes]

Manuscript submitted October 1, 2018; revised manuscript received November 13, 2018. Published November 30, 2018.

Coating metals with organic polymers presents a simple and cost-effective method of corrosion protection.[1,2] If the polymer coatings suffer discontinuities, e.g. pores or scratches, ingress of water and ions is possible. The electrolyte solution is introducing a starting point for the deadhesion of the coating.[3] One of the fastest mechanisms of failure of organic paints on iron and steels under conditions of high humidity is cathodic delamination. The delamination of polymers can be significantly slowed down by covalently linking the polymer to the metal surface, compared to films bound by van der Waals interactions.[4,5] Covalent interactions to the metal surface can also occur when a complexing agent is incorporated into a polymer coating, as e.g. shown for the example of in-coating phenyl phosphonic acid additions.[6] Cross linking of the polymer films affects e.g. water uptake of the coating, and is hence useful to slow down delamination.[4,7] For the progress of cathodic delamination, the rate of oxygen reduction at the surface is crucial,[8,9] but ion transport is important as well.[10] For the particular case of iron and mild steel, polymer covered systems have been the subject of many investigations with the aim of improving resistance to and understanding mechanism of cathodic delamination,[7,11–14] however, typically without control of the interfacial bonding between iron and the polymer.

An attractive option to tailor polymer/metal interfacial properties in order to ensure maximum stability would be to build up polymer coatings from the surface, while the polymer is also covalently linked to the metal. Polymers can be grafted from surfaces through surface initiated polymerization. A powerful technique to synthesize well-defined polymer brushes from surfaces is surface initiated atom transfer radical polymerization (SI-ATRP).[15] SI-ATRP is a living radical polymerization technique that yields polymer structures of well-defined composition.[16] SI-ATRP has extensively been used to functionalize solid inert materials with polymers for specific applications.[16] Silane and thiol compounds with -Cl or -Br containing head groups are the most extensively used as SI-ATRP initiators, especially for modifying surfaces such as oxides, gold or silicon.[17–19] Passive metals, such as nickel and stainless steels have also been coated with polymers by SI-ATRP.[20,21]

Creating anchored polymer coatings on active metals, such as iron, is challenging due to their chemical reactivity. In particular, the possibility of electrochemical reactions with the nobler copper salts contained in the most widespread ATRP catalysts is perceived as a problem.[22,23] Cold-rolled steel and iron have been used as substrates for SI-ATRP, either using an iron-based catalyst,[20] or using a macroinitiator.[22] Inevitably, the corrosion potential shifted to higher values after modification,[20,22] a consequence of removing active metal surface area. When using an *N*-bound macroinitiator, long term stability of the polymer/metal system was found to be insufficient,[22] likely because of failure of the interfacial linkage between iron and the polymer. Delamination of the produced polymer layers was not investigated systematically. Using electrografting,[23] one possible synthesis method, is of limited suitability to obtain a homogeneous polymer film which is separating the electrolyte from the active metal, as needed in a passivating coating.

Herein, the modification is reported of iron substrates with poly(methyl methacrylate) [PMMA] brushes grafted by SI-ATRP, using alkoxy and halogen silane initiators. The silane-initiator films acted as a conversion-like coating pretreatment that passivated the metal surface,[24,25] permitting use of the standard Cu-based catalyst to prepare otherwise identical polymer layers. The obtained systems were characterized mainly by infrared (IR) spectroscopy and X-ray photoelectron spectroscopy (XPS). Scanning Kelvin probe (SKP) measurements have been used to assess the rate of cathodic delamination.

Experimental

Preparation.— *Materials.*—Iron sheets (Armco Reineisen grade 4, purity 99.87%) were obtained from AK Steel GmbH (Düsseldorf, Germany). Methylmethacrylate (MMA, 99%), 2,2'-bipyridine (Bipy, 98%), triethylamine (TEA, 99%), 3-aminopropyltriethoxysilane (APTES), 2-bromoisobutyrylbromide (BIBB), copper(I) chloride (97%), copper(II) chloride (98%), copper(I) bromide (98%), copper(II) bromide (99%), tetrahydrofuran anhydrous (THF, 99.9%), toluene anhydrous (99.9%), methanol (99.8%), ethanol (99.8%), acetone (99%) were supplied by VWR. 2-(4-chlorosulfonylphenyl)ethyltrichlorosilane, (CTCS) in toluene (50%) was purchased from abcr GmbH. All chemicals were used as received.

Synthesis of 3-(α-bromo-2-methyl)propylamide propyltriethoxysilane (BMPPTS).—The preparation of BMPPTS (see Figure 1 for the

[z] E-mail: atrp-pmma-iron@the-passivists.org

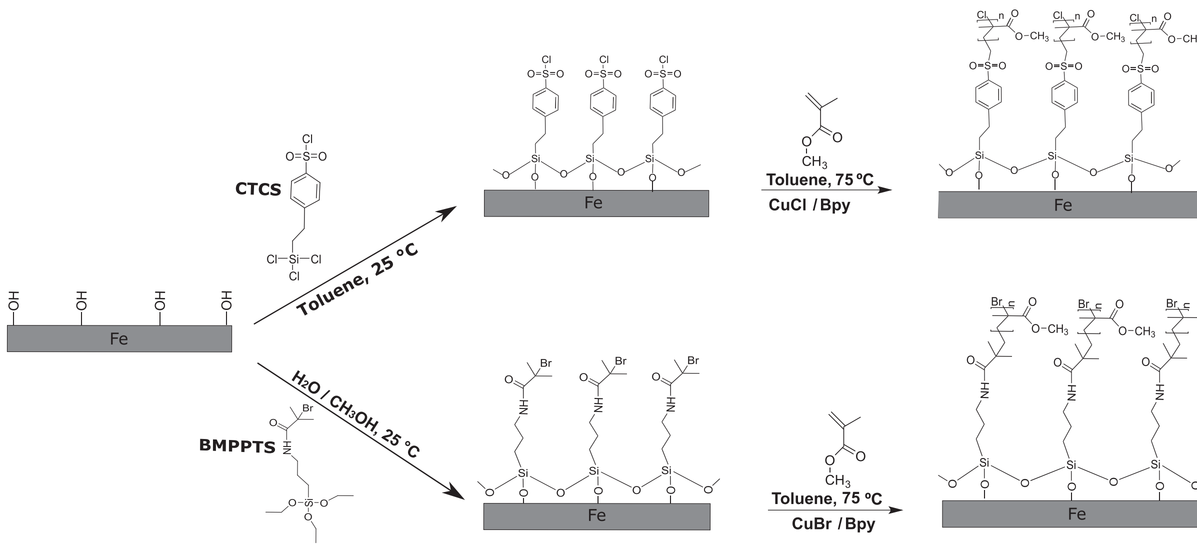

Figure 1. Schematic view of the preparation of PMMA brushes via SI-ATRP on iron using CTCS and BMPPTS as initiators. As first step of surface modification, the respective silane compound was deposited onto an iron substrate. Interface linkage is schematically shown as monolayer, however, in relality there was likely a multilayer film present. On top of the initiation "preatreatment layer", polymerization was carried out in toluene at 75°C.

structure) was carried out as reported elsewhere.[20] 50 mL of anhydrous THF were introduced into a three-necked 100 mL round bottom flask, previously immersed in an ice bath. The flask was equipped with a dropping funnel, magnetic stirrer, and was purged with an argon stream. The THF load was stirred for 15 min to let to the temperature equilibrate; immediately after that, 5 mL (36 mmol) of TEA and 7 mL (30 mmol) of APTES were added to the system under agitation. Subsequently, 4.45 mL (36 mmol) of BIBB were added dropwise trough the dropping funnel. The reaction was allowed to continue for 4 h under degasification at ambient temperature. At the end, the white solid by-product was separated by filtration and a yellowish liquid was obtained. The product was stored refrigerated and under light protection.

Surface modification of iron surfaces.—Iron coupons (15 mm × 20 mm × 4 mm) were mechanically ground with silicon carbide paper from 120 to 4000-grit, followed by polishing with silicon oxide suspension (1-2 μm) until a smooth and a mirror-like surface appearance was achieved. Thereafter, the polished samples were sonicated in ethanol for 15 min, to remove remainders of polishing suspension, and washed with copious amount of ethanol and acetone (in that order). To ensure a repeatable OH groups surface coverage on the iron surface, the coupons were immersed in solution of 0.1 M NaOH for 30 s, and immediately used for silanization.

Deposition of CTCS and BMPPTS onto iron surfaces.—In the case of CTCS, Fe-OH coupons, screwed to a homemade Teflon-stick-holder, were introduced into a Schlenk tube containing 40 mL of anhydrous toluene under agitation. After 1 h of degasification with argon, 0.5 mL (2 mmol) of CTCS were added via a syringe and the reaction was allowed to continue for 3 h at ambient temperature. At the end of the reaction, the metal coupons were dismounted and washed with copious amount of toluene, acetone, ethanol and deionized water (in that order) and dried with a nitrogen stream. The functionalized samples were stored at a reduced pressure prior to use. These samples will be referred to as Fe-CTCS. In the case of BMPPTS, a solution containing 2 parts (vol.) BMPPTS, 10 parts of methanol and 88 parts of deionized water was prepared by adding the silane compound to methanol and pouring this mixture to water. The solution was kept at 40°C for 3 h under magnetic stirring. Afterwards, Fe-OH coupons were immersed into the solution for 40 s at room temperature, followed by rinsing with copious amount of ethanol and drying with a nitrogen stream. The modified samples were stored at reduced pressure prior to use. These samples will be referred to as Fe-BMPPTS.

Polymerization of MMA from CTCS and BMPTTS initiators.—In a typical reaction using CTCS as initiator, 10 g (99.8 mmol) of MMA were diluted in 30 mL of toluene in a Schlenk tube, and the mixture was degasified with an argon stream under magnetic stirring for 1 h. Subsequently, the temperature was raised to 75°C by using an oil bath, and the CTCS-modified iron sample was introduced into the monomer solution followed by CuCl (0.05 g, 0.5 mmol), $CuCl_2$ (0.1 g, 0.074 mmol) and bipyridine (3 g, 19.2 mmol). The polymerization was conducted for 3 h in argon atmosphere under agitation. At the end of the reaction, the polymer-modified iron sample was introduced into fresh toluene, followed by rinsing with acetone and deionized water, and drying under a nitrogen stream. The procedure and the formulation to grow polymer brushes from BMPPTS initiator were identical to those utilized with CTCS. The only relevant difference is that the catalyst was changed, in this case CuBr (0.5 g, 0.34 mmol) and $CuBr_2$ (0.1 g, 0.044 mmol) were used. The amount of ligand was maintained constant. These samples will be referred to as Fe-CTCS-PMMA and Fe-BMPPTS-PMMA, respectively.

Characterization of modified iron surfaces.—Elemental composition of CTCS, BMPPTS and PMMA modified surfaces was analyzed by XPS using a Quantera II (Physical Electronics) spectrometer. The measurements were carried out at a take-off angle $\theta = 45°$, with the application of a monochromatic Al Kα X-ray source (1486.6 eV) at pass energy of 26 eV and an energy step size of 0.05 eV. Survey scans were performed in three different areas to detect elements of interest, at a pass energy of 144 eV and an energy step of 0.1 eV.

The surface coverage of initiators on the modified iron samples was determined as in a previous work.[26] Surface coverage $\Gamma(X)$ of CTCS and BMPPTS was determined from comparing the peak intensities of Si 2p and N 1s peaks, respectively, to the Fe 2p peak of the substrate as [27–29]

$$\Gamma(X) = \frac{A_X}{A_{\mathrm{Fe}}}\frac{S_{\mathrm{Fe}}}{S_X}\rho(\mathrm{Fe};\mathrm{Fe}_x\mathrm{O}_y)\lambda(\mathrm{Fe};\mathrm{Fe}_x\mathrm{O}_y)\sin(\theta)\frac{e^{d/[\lambda(X;\mathrm{Ini})\sin(\theta)]}}{e^{d/[\lambda(\mathrm{Fe};\mathrm{Ini})\sin(\theta)]}}. \quad [1]$$

The respective element peak used is represented by X. The area ratio of the peaks of X (Si 2p or N 1s) and Fe 2p is denoted as $\frac{A_X}{A_{\mathrm{Fe}}}$, while $\frac{S_{\mathrm{Fe}}}{S_X}$ represents the ratio of the respective atomic sensitivity factors. A value of $9.862 \cdot 10^{22}$ cm^{-3} was used as density $\rho(\mathrm{Fe};\mathrm{Fe}_x\mathrm{O}_y)$ of iron atoms per unit volume in Fe_xO_y.[30] The different inelastic mean free paths λ of the respective photoelectrons in the different media have been obtained as follows. In the Fe_xO_y layer, $\lambda(\mathrm{Fe}; Fe_xO_y)$ of the Fe photoelectrons was considered as 0.306 nm.[30] For Si 2p or N 1s, and Fe 2p photoelectrons in the initiator layer, $\lambda(\mathrm{Si}; \mathrm{Ini})$, $\lambda(\mathrm{N}; \mathrm{Ini})$ [for the respective $\lambda(X; \mathrm{Ini})$ in Eq. 1], and $\lambda(\mathrm{Fe}; \mathrm{Ini})$, respectively, were calculated as[27]

$$\lambda = 9.0\,\text{Å} + 0.022\,\text{Å}\,(\text{eV})^{-1} E_{\text{kin}}, \qquad [2]$$

with the measured photoelectron kinetic energy E_{kin}.

Silane and polymer modified metal surfaces were also analyzed by IR reflectance absorbance spectroscopy with a Vertex 70v Fourier transform IR spectrometer (Bruker), operated in vacuum. The obtained spectra were recorded with a spectral resolution of 4 cm^{-1} using p-polarized light with an incidence angle of 80°. The spectrometer was provided with a middle band mercury cadmium telluride detector which was cooled with liquid nitrogen 1 h prior to measuring. Previous to any modification, background spectra of polished samples were acquired. Every spectrum was obtained averaging 250 scans.

Thicknesses of the ultrathin silane and polymer layer were determined using a UV/visible ellipsometer (SE 800, Sentech Instruments) equipped with a xenon lamp light source. The data were acquired in a wavelength range of 300-800 nm with an incident angle of 70°. The layer thickness was obtained averaging measurements of three spots and modeling with a simple air/layer/iron model. Differences in ellipsometric parameters were analyzed with respect to the bare polished iron substrate. Changes in the thickness of the oxide layer on iron were not explicitly considered and may have affected the results. The refractive indexes of PMMA and SiO_2 are very close to each other, so that the consideration of silane-based initiator and polymer as a single layer is justified.

Contact angle measurements were performed using an OCA 30 goniometer (Dataphysics) at room temperature. The contact angle values were computed at a residence time of 20 s by the sessile drop method, applying a drop volume of 5 μL of deionized water.

Crucial characterization data is available online.[31]

Electrochemical evaluation of the organic layers.—Delamination experiments were carried out using a commercial scanning Kelvin probe (SKP) system from KM Soft Control (Wicinski - Wicinski GbR, Wuppertal, Germany) with a 100 μm Nickel-Chromium tip in humid air atmosphere.[32] Before each experiment, the Kelvin probe tip was calibrated to the standard hydrogen electrode (SHE) potential scale with Cu|$CuSO_4$(sat.). All electrode potentials in this work are given with reference to SHE. The samples prepared for delamination where additionally covered with poly(vinyl butyral) (PVB) by spin-coating a few drops of a solution of 5% (w/w) PVB in ethanol onto the iron coupons at 2500 rpm for 20 s to obtain a PVB layer with a thickness of ≈1 μm. Defects in the model coatings were prepared by scratching with a scalpel. The defects produced by this method are typically ≈200 μm wide and ≈2 mm long. These defects were subsequently immediately filled with 1M KCl solution, and transferred into the SKP chamber.

A control experiment was performed to investigate the role of residual copper-containing impurities on the delamination rate as follows. 25.1 mg (0.253 mmol) of CuCl and 24.7 mg (0.184 mmol) of $CuCl_2$ were thoroughly mixed in a weighting tray. This mixture was evenly spread onto an iron sample with a spatula. The iron sample was at this point already mounted on top of the spin coater. Afterwards, the 0.5 mL of the PVB solution in ethanol was placed on top of the sample. A syringe tip was then used to mix copper salt powders and PVB solutions until it appeared homogeneous. At this point, the spin coating was started. Delamination experiments were at the end conducted in the same manner as described for the main samples.

Crucial delamination data is available online.[31]

Results and Discussion

Surface modification.—The modification steps of the iron surface are depicted in Figure 1. For the preparation of one set of model coatings, the commercial anchoring initiator CTCS was utilized. For a second set of model coatings, polymer brushes were obtained by the use of BMPPTS which was synthesized by reacting APTES and BIBB.[20] Analysis of the modified surfaces by XPS and IR spectroscopy showed a successful surface modification with the initiators (Figures 2 and 3). All expected signals were observed, and the quantitative analysis follows mostly expected trends. Crucial characterization data is also available online.[31]

Figure 2a shows the surface survey spectrum of Fe-CTCS, with signals of O 1s, C 1s, Si 2p, Si 2s, S 2p, S 2s, Cl 2p, and Cl 2s at binding energies of 531.6, 284.6, 99.6, 151, 165.8, 229.1, 199.2, and 271.1 eV, respectively.[33–35] The C:S:Si ratio, determined from the C 1s, S 2p and Si 2p spectral regions, was calculated as 8.3:1:1 which is very close to the theoretical value of 8:1:1. A high resolution C 1s spectrum of Fe-CTCS is shown in Figure 2b. The peak positions were found as 286.2, 284.7 and 284.4 eV for C-S, C-C / C=C and C-Si, respectively. A ratio for C-C/H:C-S:C-Si of 5.9:1.1:1 was found (expected 6:1:1). The surface coverage was estimated as 1 molecule nm^{-2}. The IR reflection spectrum shown in the Figure 3a also confirmed the anchoring of CTCS on the iron substrate. The strong peaks appearing between 1039 and 1125 cm^{-1} are assigned to Si-O-Si and Si-O-C vibrations.[17,36,37] Stretching modes of S=O bonds were detected at 1176 and 1376 cm^{-1}.[36,38]

In the case of BMPPTS, Figure 2c shows the XP survey spectrum of the initiator on iron. Elemental peaks corresponding to the composition of the anchored substance were recorded at 530.6, 400, 284.5, 153.5, 101.1 and 71.1 eV, corresponding to the binding energies of O 1s, N 1s, C 1s, Si 2s, Si 2p and Br 3d, respectively.[33,34] The inset with high resolution spectra of Si 2p and Br 3d shows the elements only present in the initiator for SI-ATRP. The C:N:Si ratio was determined as 6.9:1:1.3, which is similar to the calculated ratio of 7:1:1. C 1s analysis (Figure 2d) showed peaks at 288.3, 286.9, 285.8, 284.7 and 283.5 eV, respectively, for N-C=O, C-O, C-N, C-C/H and C-Si. Although C-O is not present in BMPPTS, it may have originated from organic contamination or oxidation through atmospheric transfer. An intensity ratio C-C/H:C-N:C-Si:N-C=O was found of 10:1.8:1.2:1, with a significantly too large aliphatic contribution, as the expected ratio is 3:2:1:1. The large fraction of C-C/H may indicate only partial hydrolysis of the methoxy groups. The surface coverage was estimated as 1.4 molecule nm^{-2}. The IR reflection spectrum (Figure 3a) of Fe-BMPPTS also confirmed the successful anchoring of the ATRP initiator on the surface. The siloxane vibrational modes appeared between 959 and 1122 cm^{-1}. The N-H bending mode was assigned to the peak located at 1535 cm^{-1}.[39] The small peak present at 1731 cm^{-1} originates from the C=O group present in the head of the molecule.[39] The C-H stretching vibrations of the alkyl groups appeared at 2923 and 2965 cm^{-1}. OH stretching modes of strongly hydrogen bound water or hydroxyl groups were present, centered at around 3200 cm^{-1}. The presence of these modes indicates the presence of residual OH groups in the prepared layers. Discussions of the interfacial absorption spectrum of water are available elsewhere.[40,41]

Thicknesses of the surface-bound initiator layers were determined by ellipsometry as (3.7±0.6) nm and (4.1±0.4) nm for Fe-CTCS and Fe-BMPPTS, respectively. These values are slightly higher than expected for monolayer coverage, which could either indicate a crosslinking between the siloxane molecules, or an effect of changes in the iron oxide layer. Given the fact that multilayer formation is known for silanes with more than one leaving group,[42] the former possibility is quite likely. Contact angle measurements also confirmed the modification of the substrate. Polished iron samples without dip in NaOH showed contact angles of (51±3)°. After deposition of the silane initiators, contact angles increased by around 10°.

For the second step of modification, the polymerization of MMA from the initiator-functionalized iron surfaces was carried in toluene at 75°C using a copper salt based catalyst.[43] In ATRP systems, a

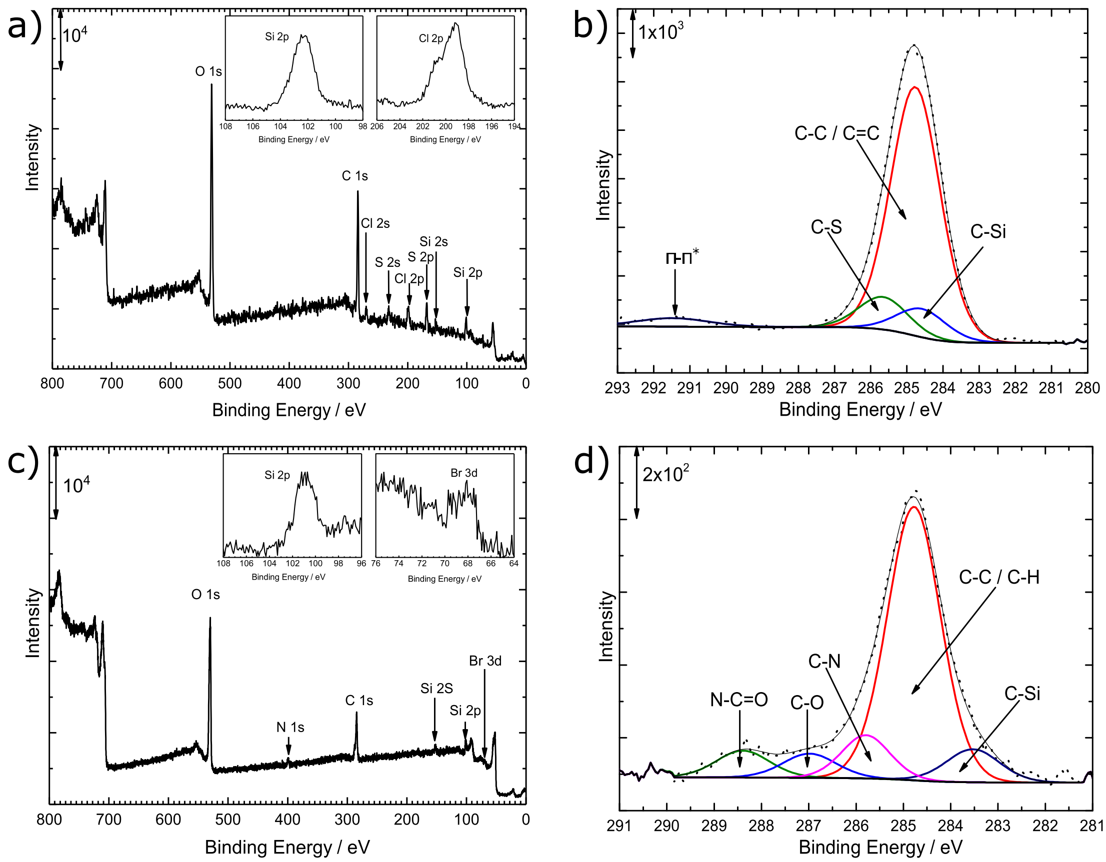

Figure 2. XPS spectra; a) survey spectrum of Fe-CTCS, with inset showing high resolution spectra of Si 2p and Cl 2p regions; b) C 1s region of Fe-CTCS; c) survey spectrum of Fe-BMPPTS with insets of the high resolution spectra of the Si 2p and Br 2p regions; d) C 1s region of Fe-BMPPTS.

"sacrificial initiator", or a sufficient amount of deactivators are required to ensure control of the radical concentration and thus avoiding termination reactions.[44] In this study, Cu^{II} was added as deactivator.[21]

The IR spectra (Figure 3a, spectra (iii) and (iv)) confirmed the successful polymerization of MMA from the initiator layers. Peaks were empirically assigned as follows.[45] The strong vibrational bands found in the range of 1151 and 1272 cm^{-1} were attributed to the vibrational modes of C-O present in the ester moieties, and delocalized modes of the whole molecules. The peaks at 1387 and 1384 cm^{-1}, respectively, correspond to the symmetric scissoring modes of methyl groups in the

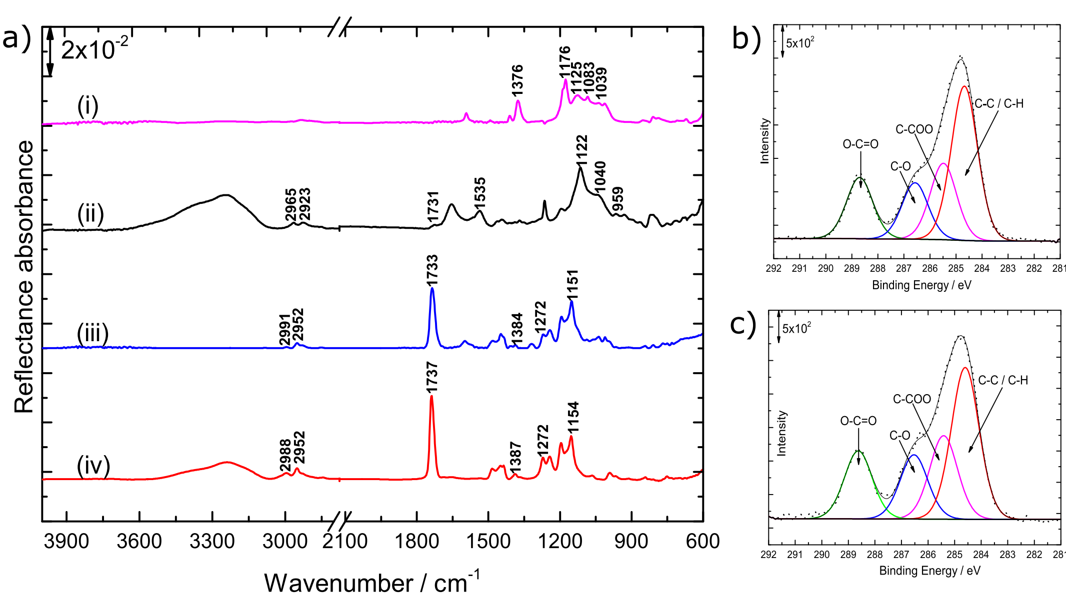

Figure 3. a) IR spectra obtained from modified iron surfaces with i) CTCS, ii) BMPPTS, iii) CTCS-PMMA and iv) BMPPTS-PMMA. b) and c) XP C 1s spectra recorded from Fe-PMMA and Fe-BMPPTS-PMMA samples, respectively.

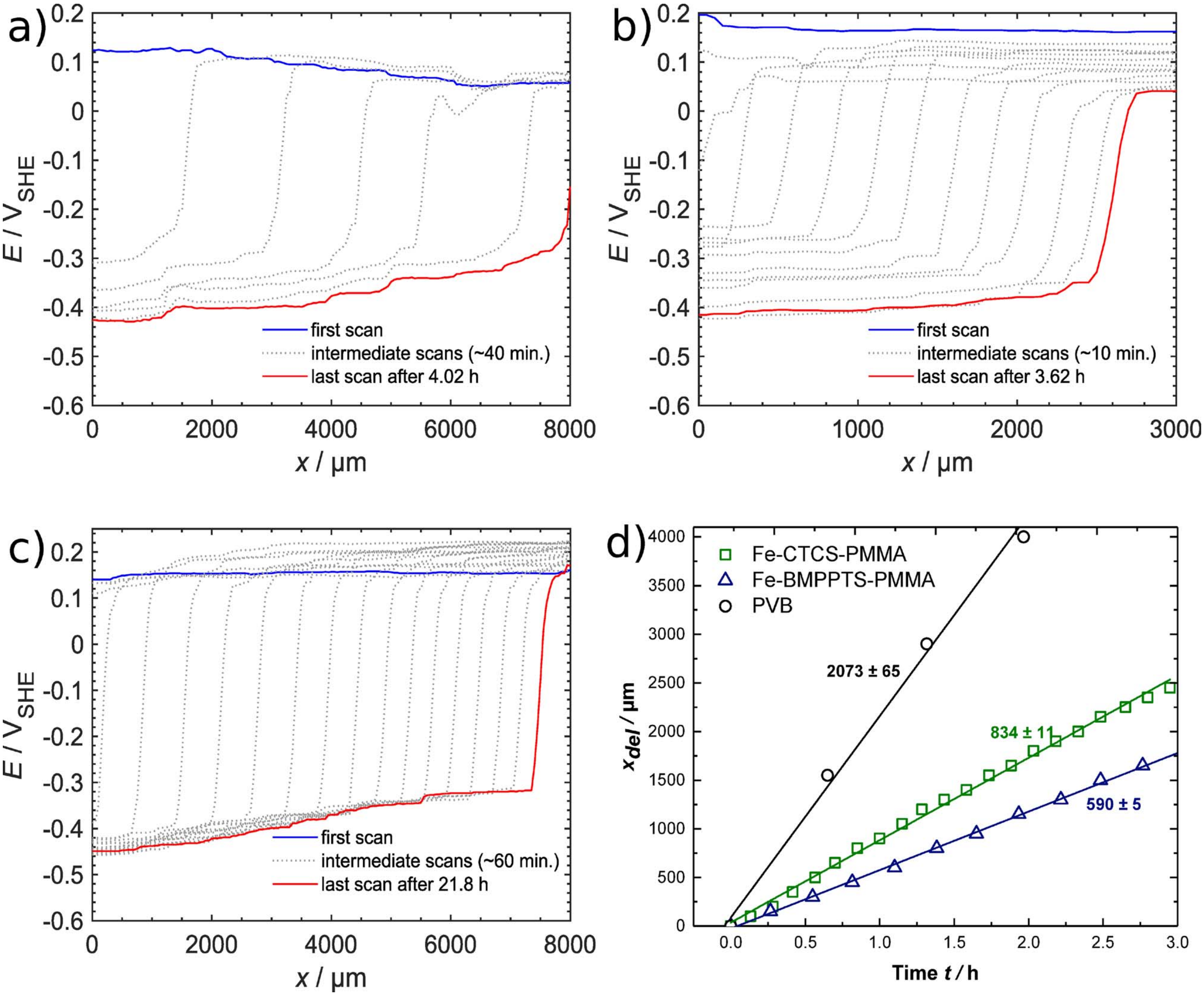

Figure 4. SKP delamination profiles of a) PVB, b) PVB covered Fe-CTCS-PBMA and c) PVB covered Fe-BMPPTS-PMMA model coatings. Defects were filled with 1 M KCl. In d), the position *x* of the delamination front (extracted from delamination profiles) is plotted as a function of time *t* of progress of the delamination experiment for one measurement of each of the model coatings. Data was extracted from the profiles in a, b and c. The indicated slopes represent the delamination rate in $\mu m\ h^{-1}$.

backbone of Fe-BMPPTS-PMMA and Fe-CTCS-PMMA. The characteristic carbonyl (C=O) stretching mode of the repeating unit was found at 1733 cm^{-1} for Fe-CTCS-PMMA and at 1737 cm^{-1} for Fe-BMPPTS-PMMA. The C-H stretching modes were detected in the typical range of 2952–2991 cm^{-1}.[45]

High resolution XP C 1s spectra for Fe-CTCS-PMMA and Fe-BMPPTS-PMMA are shown in Figure 3b and Figure 3c, respectively. The composition of the C 1s peak was in reasonable agreement with the expected composition. Figure 3b shows C 1s spectra for Fe-CTCS-PMMA. Peaks were found at 288.7, 286.6, 285.4 and 284.7 eV for O-C=O, C-O, C-COO and C-C/H, respectively. The expected intensity ratio C-C/H:C-COO:C-O:C-C=O was 2:1:1:1, considering only PMMA,[46] which is similar to the experimental value (2.7:1.3:1:1.08).

For Fe-BMPPTS-PMMA, the peaks were found at 288.6, 286.5, 285.4 and 284.6 eV for O-C=O, C-O, C-COO and C-C/H, respectively. The experimental intensity ratio C-C/H:C-COO:C-O:C-C=O was 2.3:1.3:1:1.05, reasonably close to the expected value of 2:1:1:1.[46]

The polymer film thicknesses were determined after 3 h of reaction, and found to be (38±3) nm for Fe-CTCS-PMMA and (33±4) nm for Fe-BMPPTS-PMMA. This thickness range is similar to previously reported works.[20–22] As the samples were modified with PMMA, the surface became more hydrophobic, as evidenced by contact angle measurements. Contact angles were measured as $(77\pm4)^\circ$ for Fe-CTCS-PMMA, and $(80\pm3)^\circ$ for Fe-BMPPTS-PMMA.

Stability of polymer layers.—The cathodic delamination of the grafted films was investigated by SKP. The progress of the delamination front was tracked from an artificial defect filled with 1 M KCl. Progress of the delamination front was analyzed as described elsewhere.[47,48] For the measurements, the polymer-grafted samples were covered with a ≈1 µm thick, spin-coated PVB top layer to avoid electrolyte spreading above the PMMA modified surface.[4,49] Sample sets were assessed simultaneously in the SKP chamber, i.e. exposed to the same environment with the aim to avoid interference due to variations of oxygen partial pressure or relative humidity. Three different systems were tested: i) a non-covalently bound coating of PVB spin-coated on bare iron, ii) Fe-CTCS-PMMA and iii) Fe-BMPPTS-PMMA grafted films. As the thickness of the top PVB layer was significantly larger than the thickness of the grafted polymer layer, effects of the different layer thicknesses should be leveled out by the presence of PVB.

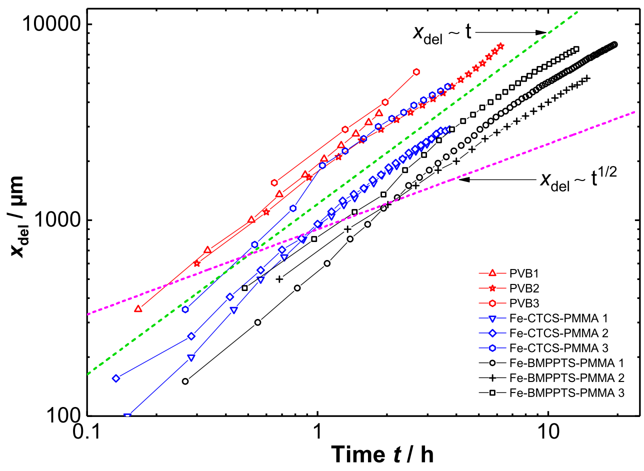

Figure 5. Progress of delamination front with time for Fe-CTCS-PMMA (blue) and Fe-BMPPTS-PMMA (black), in comparison to reference measurements with PVB on iron (red). For reference, lines with the slopes of 1 and 1/2 are given, representing different exponents α of the time dependence power law $x \propto t^{\alpha}$. Observed slopes are summarized in Table I.

Figures 4a–4c shows the detected potential distributions for samples of the evaluated model coatings. (Data is available online.[31]) Two potential levels characterized the delamination profiles: −300 to −500 mV corresponding to the defect region, and 0 and 200 mV belonging to the area with intact model coating.[3,50,51] The latter was related to the oxide present at the interface,[52] while the former was the open circuit potential of corroding iron in chloride containing aqueous solutions.[52] As delamination progressed, the potential of a previously intact region was shifted toward the defect potential. The midpoint between the defect and the intact potential was treated as the position x of the delamination front. Around the delamination front, quite complex chemical processes can happen, as solvent availability and oxygen availability are limited.[53] As the delamination front progressed, the potential distribution in the delaminated area shifted to more positive values. This shift reflected changes in the reaction conditions at the interface owing to ohmic potential drops.[48,51]

Figure 5 displays the delamination front position x as function of time t of the delamination experiment on a double logarithmic scale. Time 0 was taken as the time before the first shift in the potential profile was observed. The double logarithmic plot facilitated a determination of the exponent α of the time dependence $x \propto t^{\alpha}$. A value of $\alpha = 1/2$ has been widely reported for the delamination of polymers on iron and associated with rate control by a diffusion process,[48,50,52,54] while $\alpha = 1$ was associated with a reaction controlled rate.[4] In self-healing systems, $\alpha \to 0$ after a certain time.[13,55] Figure 5 shows that in this work, some series approach $\alpha = 1/2$ at large times. For most of the duration of the experiments, $\alpha \approx 1$.

Because the potential difference between the delaminated area and the intact coating is the driving force for delamination processes,[12] the early delamination stage is especially important; the disbonding rate of the polymer occurs faster at this region, in comparison with regions away from the defect.[56,57] These results were plotted on a linear scale and are shown in Figure 4d. The slope in the initial phase of the $x(t)$ curve is the initial delamination rate (Table I). Polymers bound to iron by BMPPTS showed consistently the slowest delamination, and weakly bound PVB showed the highest. CTCS-bound layers showed a relatively large spread. One series was similar to the control with PVB, while others resembled more closely the time-dependence of Fe-BMPPTS-PMMA. Overall, Fe-BMPPTS-PMMA showed the lowest delamination rate and the lowest relative uncertainty in this series.

It should be stressed here that in a previous study of delamination of PMMA prepared by free radical polymerization on zinc,[4] the largest part of the decrease in delamination rate originated from the bifunctional siloxane layer. Surface modification of zinc only with

Table I. Initial delamination rates and exponents α of the time dependence $x \propto t^{\alpha}$ during cathodic delamination of the differently initiated polymers deposited on iron. Uncertainties represent the single standard deviation from three repeats of the experiment.

Sample	α	Initial delamination rate/mm h^{-1}
PVB	0.89 ± 0.07	1.7 ± 0.4
Fe-CTCS-PMMA	1.03 ± 0.02	1.0 ± 0.3
Fe-BMPPTS-PMMA	0.84 ± 0.07	0.6 ± 0.1

vinyltrimethoxysilane reduced the delamination rate to ≈5% of that of the PVB reference system. The PMMA on top led to an additional ≈50% reduction, whereas a further reduction was achieved by crosslinking.[4] In the more hydrophobic poly(styrene) system on zinc, the effect of crosslinking was more involved.[58] While the initiator alone has not been investigated here, based on the experience from the Zn-PMMA system, a significant effect is to be expected here as well. In particular, an investigation of several acrylates on iron showed that PMMA alone is an extremely weak coating, weaker even than PVB.[14] It is therefore expected on that basis that purely linear PMMA does not contribute a lot to slowing down delamination. The additional effect observed in the zinc system may hence be related to crosslinking via side reactions in the polymerization process performed in that work.[4]

One factor that could have led to a fast delamination at the interface is the presence of metallic copper, forming by cementation of the Cu from the catalyst system on the less noble iron surface. This hypothesis was, however, excluded by a control experiment. An iron surface was contaminated with copper salts containing both Cu^{I} and Cu^{II}, coated with PVB in the same manner as the other samples, an subjected to a delamination experiment. A mixture of Cu^{I} and Cu^{II} salts was used, as copper is present in two oxidation states in the catalyst system as well. The amount of copper salts put on the surface was ca. 1.4 mol m^{-2}, and thus 30% lower than but in the same order of magnitude as expected if the complete amount of Cu present in the polymerization solution would cement on the iron surface. The latter process would yield ≈2 mol m^{-2}. On the other hand, the surface concentration of expected active polymerization sites would at maximum be on the order of 1 µmol m^{-2}, based on the determined surface coverage of 1 molecule nm^{-2}. Low levels of Cu such as residuals from the active polymerization chains in the final coatings may thus have completely different effects, and their presence cannot be ruled out with the conducted experiment. The delamination profile of this experiment is shown in Figure 6. The result showed a very inhomogeneous potential profile, which was likely caused by metallic copper islands on the surface. Cu islands are supposed to show a significantly different potential than iron. Such inhomogeniety in the potential profiles was not observed for the prepared model coatings. Overall progress of the delamination in copper-contaminated iron was also surprisingly only half as large the comparative PVB case.

The large spread, and the differences between CTCS and BMPPTS as initiators may have been related to the possibility that CTCS may have bound to the surface in a diffent geometry than expected, e.g. with the sulfonate group, deactivating the catalytically required S-Cl bond. The fact that surface bound polymers with reasonable thickness were obtained does, however, also exclude loss of active sites for polymerization on the majority of the surface.

Differences in surface coverage may also have led to differences in the observed delamination rates between the different polymers. CTCS surface coverage was estimated as 1 molecule nm^{-2}, whereas BMPPTS coverage was 1.4 molecule nm^{-2}, as determined by XPS. This result would already suggest a slower delamination of the system with a higher initiator density. However, different XPS peaks were used in the surface coverage determination, and the typical assumptions were made regarding the calculation of the inelastic mean free path. It is therefore not entirely clear if the obtained difference is quantitatively reliable. On the other hand, the initiator layer thickness

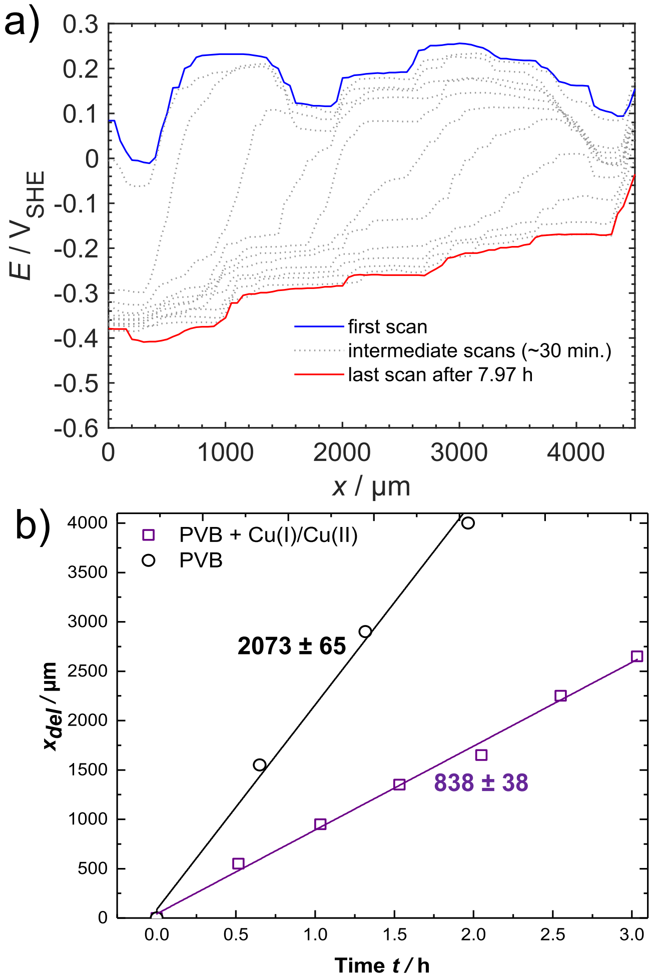

Figure 6. Delamination profiles of a) PVB on Fe with copper contamination prepared as described in the experimental section. b) Delamination front position x_{del} versus delamination time t for cases of pure PVB, Figure 4a, and the copper contaminated sample shown in this figure. The indicated slopes represent the delamination rate in $\mu m\ h^{-1}$.

was identical within single standard deviation for the two systems investigated here, suggesting that a lower value in organic surface coverage is compensated by a larger amount of siloxanes. This interpretation agrees with the traces of non-hydrolyzed silane found for BMPPTS. Finally, the thicknesses of the polymerized layers also agreed within single standard deviations between the systems investigated. Differences in coverage may therefore have contributed to the observed differences in delamination rates, but are unlikely to have been decisive.

A further possible reason for the observed fast delamination of some Fe-CTCS-PMMA samples is the presence of chloride at the polymer/metal interface, as residue from the initiator. Si-Cl groups may be insufficiently hydrolyzed during the surface modification process. Given the reactivity of the Si-Cl bond, insufficient hydrolysis is considered to be unlikely. More likely is a remaining presence of chloride at the interface after hydrolysis, e.g. also surface-bound to iron. From investigating adsorbed low-molecular weight compounds, some studies have concluded that chlorosilanes are not suitable for application in corrosion protection,[21,59] while in other cases beneficial effects have been reported.[59,60] The discrepancy is likely caused by the practical difficulty to control the residual amount of chloride at the interface. The use of alkoxysilanes circumvents this difficulty.

For Fe-BMPPTS-PMMA, a significant slow-down of cathodic delamination was observed. In this system, ion migration is hindered by the covalent interfacial bonds at the BMPPTS-PMMA/Fe interface. In cathodic delamination, oxygen reduction produces hydroxide, consequently generating a pH gradient along the polymer/metal interface, where an alkaline pH is observed at the delamination front.[37] At a pH above 10, Si-O bonds may undergo hydrolysis.[61] Such pH values can easily be reached as consequence of oxygen reduction. Hydrolysis, or reactions with radical intermediates, may thus contribute to the delamination.[4]

Conclusions

Model coatings with a well-defined linkage to iron were prepared using SI-ATRP and used as models to investigate cathodic delamination. The use of the conventional ATRP copper-based catalyst was not problematic in that sense that delamination of model coatings was not accelerated. On the other hand, chloride-containing precursors of the surface-bound initiator likely left chloride remnants at the iron/polymer interface. The latter enhanced delamination in subsequent experiments. With alkoxy-based initiators, this problem was solved, and a reduction in the delamination rate was obtained. It cannot be ruled out that differences in the initiator layer structure, such as packing density, contributed to the observed differences. It is likely that the alkoxysilane-based initiators work similar as a modern sol/gel conversion coatings, first of all by passivating the surface. This chemistry shows room for further development of passivating coatings.

Acknowledgment

J.S.M.O. thanks the Mexican Consejo Nacional de Ciencia y Tecnología (CONACYT) for a scholarship. A.A. and A.E. acknowledge the DFG (Deutsche Forschungsgemeinschaft) for the financial support via the subproject ER 601/3-1 within priority program 1640 "Joining by plastic deformation". The authors thank Michael Rohwerder for fruitful discussions and M. Stratmann for continuous support.

ORCID

Andreas Erbe https://orcid.org/0000-0001-7840-2585

References

1. O. Ø. Knudsen and A. Forsgren, *Corrosion Control Through Organic Coatings*, Second Edition, CRC Press, Boca Rayton, USA (2017).
2. G. Grundmeier and A. Simões, *Encyclopedia of Electrochemistry*, vol. 4, chap. Corrosion Protection by Organic Coatings, 500–566. Wiley-VCH, Weinheim, Germany (2003).
3. A. Leng, H. Streckel, and M. Stratmann, *Corros. Sci.*, **41**, 547 (1998).
4. D. Iqbal, J. Rechmann, A. Sarfraz, A. Altin, G. Genchev, and A. Erbe, *ACS Appl. Mater. Interfaces*, **6**, 18112 (2014).
5. M. Santa, R. Posner, and G. Grundmeier, *J. Electrochem. Soc.*, **158**, C36 (2011).
6. C. F. Glover, R. Subramanian, and G. Williams, *J. Electrochem. Soc.*, **162**, C433 (2015).
7. R. Posner, P. E. Sundell, T. Bergman, P. Roose, M. Heylen, G. Grundmeier, and P. Keil, *J. Electrochem. Soc.*, **158**, C185 (2011).
8. D. Vijayshankar, A. Altin, C. Merola, A. Bashir, E. Heinen, and M. Rohwerder, *J. Electrochem. Soc.*, **163**, C778 (2016).
9. N. Wint, S. Geary, H. N. McMurray, G. Williams, and A. C. A. de Vooys, *J. Electrochem. Soc.*, **162**, C775 (2015).
10. R. Posner, M. Santa, and G. Grundmeier, *J. Electrochem. Soc.*, **158**, C29 (2011).
11. S. H. Cho, S. R. White, and P. V. Braun, *Adv. Mater.*, **21**, 645 (2009).
12. G. Paliwoda-Porebska, M. Stratmann, M. Rohwerder, K. Potje-Kamloth, Y. Lu, A. Z. Pich, and H. J. Adler, *Corros. Sci.*, **47**, 3216 (2005).
13. A. Vimalanandan, L.-P. Lv, T. H. Tran, K. Landfester, D. Crespy, and M. Rohwerder, *Adv. Mater.*, **25**, 6980 (2013).
14. J. S. Mondragón Ochoa, A. Altin, and A. Erbe, *Mater. Corros.*, **68**, 1326 (2017).
15. A. Khabibullin, E. Mastan, K. Matyjaszewski, and S. Zhu, Surface-initiated atom transfer radical polymerization. In P. Vana (Ed.), *Controlled Radical Polymerization at and from Solid Surfaces*, vol. 270, 29–76. Springer, Cham, Switzerland (2015).
16. K. Matyjaszewski and N. V. Tsarevsky, *Nat. Chem.*, **1**, 276 (2009).
17. I. Garcia, N. E. Zafeiropoulos, A. Janke, A. Tercjak, A. Eceiza, M. Stamm, and I. Mondragon, *J. Polym. Sci., Part A-1: Polym. Chem.*, **45**, 925 (2007).
18. J.-B. Kim, M. L. Bruening, and G. L. Baker, *J. Am. Chem. Soc.*, **122**, 7616 (2000).
19. S. Ding, J. A. Floyd, and K. B. Walters, *J. Polym. Sci., Part A-1: Polym. Chem.*, **47**, 6552 (2009).
20. R. Gong, S. Maclaughlin, and S. Zhu, *Appl. Surf. Sci.*, **254**, 6802 (2008).
21. R. Chen, S. Zhu, and S. Maclaughlin, *Langmuir*, **24**, 6889 (2008).

22. G. Lu, Y.-M. Li, C.-H. Lu, and Z.-Z. Xu, *Colloid Polym. Sci.*, **288**, 1445 (2010).
23. M. Claes, S. Voccia, C. Detrembleur, C. Jérôme, B. Gilbert, P. Leclère, V. M. Geskin, R. Gouttebaron, M. Hecq, R. Lazzaroni, and R. Jérôme, *Macromolecules*, **36**, 5926 (2003).
24. A. Khramov, V. Balbyshev, N. Voevodin, and M. Donley, *Prog. Org. Coat.*, **47**, 207 (2003).
25. S. M. Jacob, United States Pat. 5053081 (1991).
26. J. Rechmann, A. Sarfraz, A. C. Götzinger, E. Dirksen, T. J. J. Müller, and A. Erbe, *Langmuir*, **31**, 7306 (2015).
27. H. Kim, P. E. Colavita, P. Paoprasert, P. Gopalan, T. Kuech, and R. J. Hamers, *Surf. Sci.*, **602**, 2382 (2008).
28. P. Paoprasert, J. E. Laaser, W. Xiong, R. A. Franking, R. J. Hamers, M. T. Zanni, J. R. Schmidt, and P. Gopalan, *J. Phys. Chem. C*, **114**, 9898 (2010).
29. P. Paoprasert, J. W. Spalenka, D. L. Peterson, R. E. Ruther, R. J. Hamers, P. G. Evans, and P. Gopalan, *J. Mater. Chem.*, **20**, 2651 (2010).
30. B. Lesiak, A. Jablonski, J. Zemek, P. Jiricek, and M. Čerňanský, *Appl. Surf. Sci.*, **252**, 330 (2005).
31. J. S. Mondragón Ochoa, A. Altin, J. Rechmann, and A. Erbe. Data for: Delamination kinetics of poly(acrylate) model coatings prepared by surface initiated atom transfer radical polymerization on iron. EDMOND - Max Planck Digital Library, https://edmond.mpdl.mpg.de/imeji/collection/4Lh9G7Y_YjYWqQ9g (2018).
32. G. S. Frankel, M. Stratmann, M. Rohwerder, A. Michalik, B. Maier, J. Doora, and M. Wicinski, *Corros. Sci.*, **49**, 2021 (2007).
33. Thermo Scientific. XPS Simplified. https://xpssimplified.com/.
34. C. Wagner, A. Naumkin, A. Kraut-Vass, J. Allison, C. Powell, and J. Rumble Jr., *NIST X-ray photoelectron spectroscopy database; NIST standard reference database 20, version 3.5 (Web version)*. NIST, Gaithersburg (2007).
35. S. Yuan, F. Xu, S. Pehkonen, Y. Ting, K. Neoh, and E. Kang, *Biotechnol. Bioeng.*, **103**, 268 (2009).
36. Z. Xu, Q. Liu, and J. Finch, *Appl. Surf. Sci.*, **120**, 269 (1997).
37. C. D. Fernández-Solis, A. Vimalanandan, A. Altin, J. S. Mondragón-Ochoa, K. Kreth, P. Keil, and A. Erbe, Fundamentals of electrochemistry, corrosion and corrosion protection. In R. P. Lang and Y. Liu (Eds.), *Lect. Notes Phys.*, vol. 917, chap. 2 - Fundamentals of Electrochemistry, Corrosion and Corrosion Protection, 29–70. Springer, Cham, Switzerland (2016).
38. P. Pacher, A. Lex, V. Proschek, O. Werzer, P. Frank, S. Temmel, W. Kern, R. Resel, A. Winkler, C. Slugovc, R. Schennach, G. Trimmel, and E. Zojer, *J. Phys. Chem. C*, **111**, 12407 (2007).
39. Z. Lei, J. Gao, X. Liu, D. Liu, and Z. Wang, *ACS Appl. Mater. Interfaces*, **8**, 10174 (2016).
40. F. Niu, R. Schulz, A. Castaeda Medina, R. Schmid, and A. Erbe, *Phys. Chem. Chem. Phys.*, **19**, 13585 (2017).
41. F. Niu, M. Rabe, S. Nayak, and A. Erbe, *J. Chem. Phys.*, **148**, 222824 (2018).
42. P. Niehoff, P. Ebbinghaus, P. Keil, and A. Erbe, *Appl. Surf. Sci.*, **258**, 3191 (2012).
43. K. Matyjaszewski and J. Xia, *Chem. Rev.*, **101**, 2921 (2001).
44. D. Zhou, X. Gao, W.-j. Wand, and S. Zhu, *Macromolecules*, **45**, 1198 (2012).
45. R. A. Nyquist, *Interpreting Infrared, Raman, and Nuclear Magnetic Resonance Spectra*, Academic Press, San Diego (2001).
46. T. Gross, A. Lippitz, W. Unger, C. Wöll, G. Hähner, and W. Braun, *Appl. Surf. Sci.*, **68**, 291 (1993).
47. M. Hernández, F. Galliano, and D. Landolt, *Corros. Sci.*, **46**, 2281 (2004).
48. M. Stratmann, R. Feser, and A. Leng, *Electrochim. Acta*, **39**, 1207 (1994).
49. C. Fernández-Solis and A. Erbe, *Biointerphases*, **11**, 021001 (2016).
50. A. Leng, H. Streckel, and M. Stratmann, *Corros. Sci.*, **41**, 579 (1998).
51. A. Leng, H. Streckel, K. Hofmann, and M. Stratmann, *Corros. Sci.*, **41**, 599 (1998).
52. J. Wielant, R. Posner, R. Hausbrand, G. Grundmeier, and H. Terryn, *Corros. Sci.*, **51**, 1664 (2009).
53. D. Iqbal, A. Sarfraz, M. Stratmann, and A. Erbe, *Chem. Commun.*, **51**, 16041 (2015).
54. W. Fürbeth and M. Stratmann, *Prog. Org. Coat.*, **39**, 23 (2000).
55. A. Altin, M. Rohwerder, and A. Erbe, *J. Electrochem. Soc.*, **164**, C128 (2017).
56. G. Williams and H. N. McMurray, *J. Electrochem. Soc.*, **148**, B377 (2001).
57. R. M. Souto, Y. González-García, J. Izquierdo, and S. González, *Corros. Sci.*, **52**, 748 (2010).
58. D. Iqbal, J. Rechmann, A. Bashir, A. Sarfraz, A. Altin, and A. Erbe, *Mater. Corros.*, DOI: 10.1002/maco.201810395 (2018).
59. D. Wang, Y. Ni, Q. Huo, and D. E. Tallman, *Thin Solid Films*, **471**, 177 (2005).
60. M. Wolpers, M. Stratmann, H. Viefhaus, and H. Streckel, *Thin Solid Films*, **210−211**, 592 (1992).
61. S. Marcinko and A. Y. Fadeev, *Langmuir*, **20**, 2270 (2004).